CORROSION RESISTANCE OF ZK40 MAGNESIUM ALLOYS MODIFIED WITH INDIVIDUAL RARE EARTH ELEMENTS AND CALCIUM OXIDE ADDITION

***R.H. Buzolin*[1,2,3], *M. Mohedano*[3,4], *C. Blawert*[3], *C.L. Mendis*[3,5], *H. Pinto*[6], *N. Hort*[3]**

[1]Christian Doppler Laboratory for Design of High-Performance Alloys by Thermomechanical Processing, 8010 Graz, Austria, ricardo.buzolin@tugraz.at
[2]Institute of Materials Science, Joining and Forming at Graz University of Technology, 8010 Graz, Austria
[3]Magnesium Innovation Centre, Helmholtz-Zentrum Geesthacht, D 21502, Geesthacht, Germany
[4]Departamento de Ingeniería Química y de Materiales, Facultad de Ciencias Químicas, Universidad Complutense, 28040 Madrid, Spain
[5]Brunel Centre for Advanced Solidification Technology, Brunel University London, Middlesex EB8 3PH, Uxbridge, UK
[6]Department of Materials Engineering, University of Sao Paulo, 13563-120, Sao Carlos, Brazil

Abstract: The effect of individual additions of calcium oxide (CaO), Gd, Nd and Y was investigated on the microstructure and corrosion resistance of the as-cast ZK40 alloy. The microstructural features were analysed using scanning electron microscopy. Electrochemical Impedance Spectroscopy, hydrogen evolution and weight loss under immersion in 0.5 wt.% NaCl solution were used to evaluate the corrosion behaviour. The corrosion behaviour was enhanced with the addition of CaO and Gd. The addition of Nd is detrimental to the corrosion resistance of the ZK40. More general corrosion is observed for the ZK40-CaO, while severe localised corrosion occurs for the ZK40-Nd.

Keywords: magnesium alloys, corrosion resistance, rare earth, calcium oxide, hydrogen evolution.

1. INTRODUCTION.

Mg alloys are lightweight structural materials with promising applications in the automotive and aerospace industry. However, Mg alloys usually have relatively low corrosion resistance, which is one of the main obstacles that impede their use [1]. Several approaches have been developed to enhance the corrosion resistance of Mg alloys. The effect of the addition of rare earth on the corrosion behaviour has yet not been fully understood [2]. Compared with the AZ alloys, the eutectic phases in ZE41 are reported not to play the role of corrosion barrier retarding the progress of the corrosion [3]. The small addition of rare earth (RE) elements to the ZK alloys can alter the microstructure and therefore can modify the mechanical properties and give satisfactory corrosion resistance. It is reported that the addition of rare-earth (RE) elements and alkaline metals to Mg alloys improves the corrosion resistance [4],[5]. Ca enhances the corrosion resistance of Mg alloys through the modification of the oxide layer [6], [7]. However, the increase of Ca additions significantly influences the anodic and cathodic polarisation to the detriment of the corrosion resistance [8]. This work investigates the role of individual rare earth elements as well as CaO on the corrosion resistance of ZK series alloys. The microstructural features are correlated to the corrosion behaviour.

2. EXPERIMENTAL PROCEDURE.

The alloys were prepared with pure Mg, Zn, CaO, Nd and master alloys Mg 10 wt.% Y, Mg 4 wt.% Gd and Mg-33 wt.%Zr (Zirmax®). Mg was molten in an electric resistance furnace and held at 750 °C, and alloying elements were added to the melt and stirred for 10 min. The melt was then poured into a preheated thin-walled steel mould held at 660 °C for 15 min. Then, the mould was immersed into at a rate of 10 mm/s until the top of the melt was in line with the cooling water. The ingots had a bottom diameter of 250 mm and a height of 300 mm. The indirect casting procedure was adopted to provide a homogeneous microstructure [9]. Table 1 shows the actual compositions of the alloys prepared for this investigation measured with X-ray fluorescence (Zn and Gd) and spark analyser (Ca, Cu, Fe, Nd, Ni, Y, Zr).

Table 1. Chemical compositions of the investigated alloys. 'ADD' corresponds to Ca, Gd, Nd and Y for the corresponding alloys. Fe, Cu and Ni are given in ppm. Other elements are provided in wt.%.

Alloys	Zn	Zr	'ADD'	Fe	Cu	Ni
ZK40	5.0	0.53	-	11	14	13
ZK40-CaO	4.4	0.34	1.2	14	16	14
ZK40-Gd	4.5	0.55	1.7	7	29	<30
ZK40-Nd	4.7	0.55	2.5	11	15	28
ZK40-Y	4.10	0.33	1.12	4	29	<2

Conventional metallographic observations was performed with a final polishing using OPS with 1 µm diamond suspension. The samples for hydrogen evolution, weight loss and impedance were not encapsulated and grounded to P2500, without polishing. Scanning electron microscopy (SEM) was performed using a Zeiss FEG-SEM Ultra 55 and a Tescan Vega3 SEM using BSE and SE electron mode operating at 15 kV. The area fraction of precipitate was determined using a minimum of five BSE micrographs analysed using the software ImageJ®.

Hydrogen evolution measurements were performed in 0.5 wt.% NaCl naturally-aerated solution for up to 10 days for the ZK40, ZK40-CaO, ZK40-Gd and ZK40-Y alloys. Due to the fast corrosion of the ZK40-Nd, the experiments were interrupted after 4 days. Immersion tests were performed for 4 h, and 24 h in 0.5 wt.% NaCl naturally-aerated solution in order to investigate the initiation of the corrosion process. The corroded surface was investigated with SEM after the removal of the corrosion products by cleaning in a solution containing 200 g/L CrO_3 at room temperature for 5-10 min following the ASTM standard G1-90, Designation C5.2. Weight loss measurements were performed after immersion for 10 days for the ZK40, ZK40-CaO, ZK40-Gd and ZK40-Y and for 4 days for the ZK40-Nd. The selected times are identical to the hydrogen evolution for comparison. The total area of the specimens was measured before the experiment. The specimens were cleaned in a solution containing 200 g/L CrO_3 at room temperature for 5-10 min. The specimens were weighed before and after the tests using a Sartorius Ax224 balance with a resolution of 0.001 g.

A Gill AC computer-controlled potentiostat was used for the electrochemical tests conducted in a stirred aqueous 0.5 wt.% NaCl solution at 22 ± 0.5°C. A typical three-electrode cell was used with the specimen as the working electrode (0.5 cm^2 exposed area), a saturated Ag/AgCl electrode as the reference electrode, and a platinum mesh as a counter electrode. Electrochemical impedance spectroscopy (EIS) measurements were performed for immersion times ranging from 1 h to 24 h at room temperature. The frequency range used was from 0.01 Hz to 30 kHz, and 10 mV RMS with respect to the OCP with an amplitude of the sinusoidal potential signal was used.

3. RESULTS AND DISCUSSION.

The SEM micrographs, illustrating the volume fraction and distribution of the intermetallic particles, are shown in Figure 1. The volume fraction of the second phases is 1.6 ± 0.5%, 6.5 ± 0.9%, 5.7 ± 1.0%, 7.3 ± 0.6% and 3.1 ± 0.5% for ZK40, ZK40-CaO, ZK40-Gd, ZK-Nd and ZK40-Y, respectively. segregation of Zn is observed from the centre of grains to the intermetallic area as illustrated by the brighter regions close to the grain boundaries, Figure 7(a). The ZK40-CaO, ZK40-Gd, ZK40-Nd and ZK40-Y alloys contain a semi-continuous distribution of intermetallic particles along the grain boundaries. In the ZK40-CaO and the ZK40-Nd, the interconnectivity is larger than the other alloys.

Figure 2 shows the volume of hydrogen evolution of investigated alloys in 0.5 wt.% NaCl. ZK40-Nd alloy evolved a considerably higher hydrogen volume compared with the other alloys. ZK40-Y showed a large hydrogen volume evolved in the first days of experiments and a notable decrease after 3 days. The evolved volume of hydrogen is the lowest for the ZK40-CaO and ZK40-Gd alloys for all measured immersion times.

Figure 3 shows the weight loss measurements after immersion in 0.5 wt.% NaCl solution for 10 days (ZK40, ZK40-CaO, ZK40-Gd and ZK40-Y) and after 4 days (ZK40-Nd). The poor corrosion resistance of the ZK40-Nd is evidenced by the highest value of corrosion rate (28.4 mg/day). The ZK40-CaO shows the lowest value (7.4 mg/day), nearly half of the ZK40, ZK40-Gd and ZK40-Y.

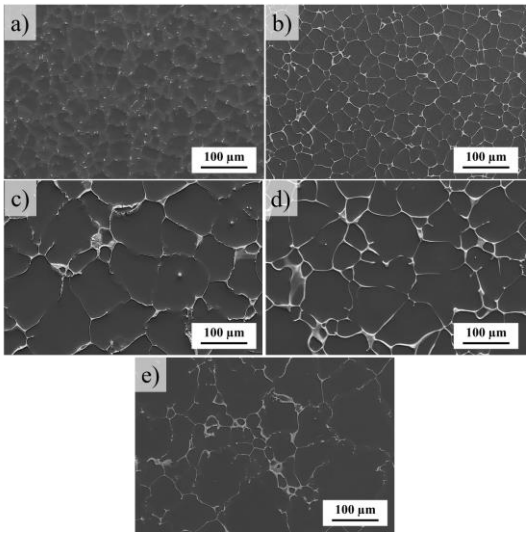

Figure 1. SEM micrographs of the as-cast alloys: a) ZK40, b) ZK40-CaO, c) ZK40-Gd, d) ZK40-Nd, e) ZK40-Y.

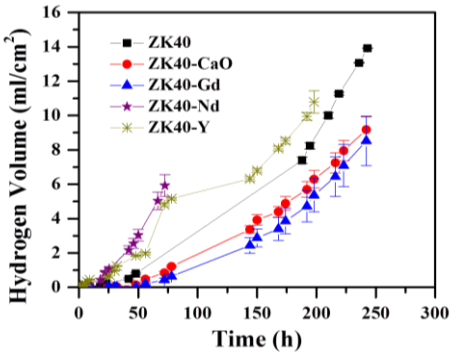

Figure 2. Volume of evolved Hydrogen during immersion in of 0.5 wt.% NaCl solution at room temperature for alloys investigated.

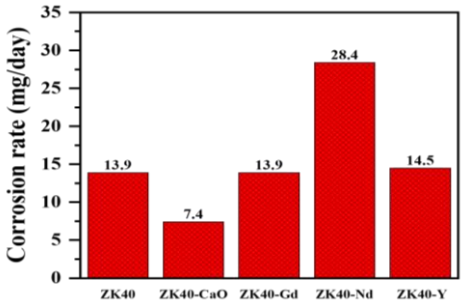

Figure 3. Corrosion rate from weight loss measurement after 10 days (ZK40, ZK40-CaO, ZK40-Gd and ZK40-Y) and 4 days (ZK40-Nd).

Figure 4 shows the Bode plots of the EIS measurement after 1 h and 24 h of immersion in 0.5 wt.% NaCl solution. The small magnitude of the impedance evidence the low corrosion resistance of the ZK40-Nd. Comparable values are observed for the ZK40-CaO and ZK40-Gd and are higher than the other alloys. Despite the increase in the thickness of the corrosion products,

localisation of corrosion and the constant disruption of the non-cohesive corrosion products are the reason for the decrease in impedance with an increase in immersion time.

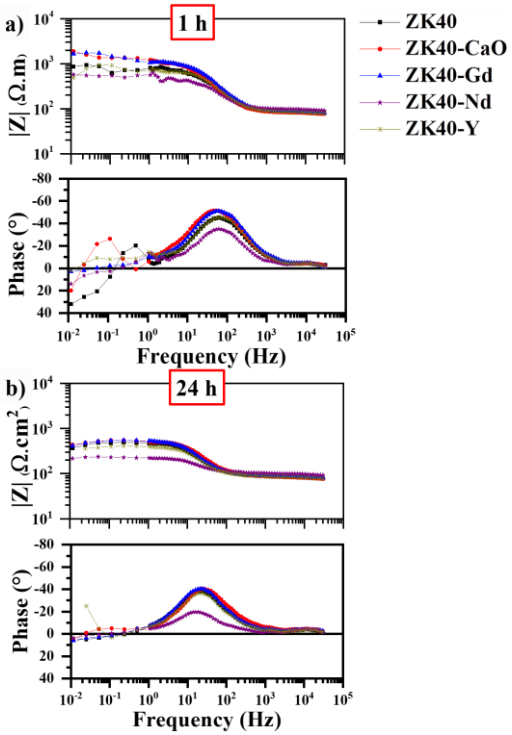

Figure 4. Measured Bode plots after immersion in 0.5 wt.% NaCl naturally aerated solution at room temperature after: a) 1 h immersion; b) after 24 h immersion.

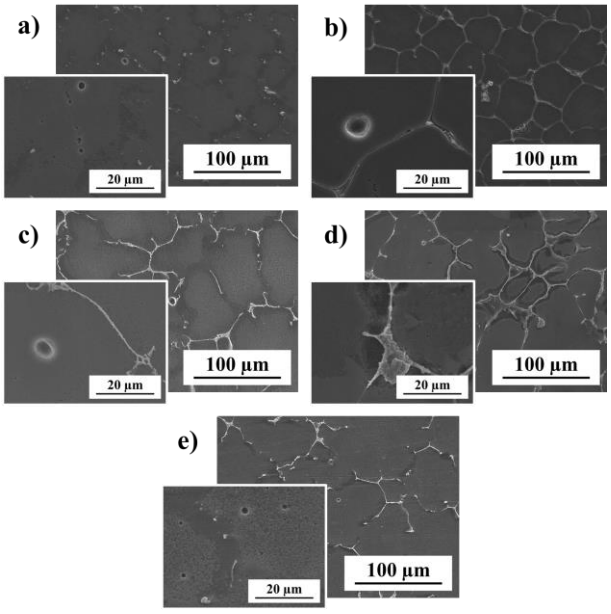

Figure 5. Corrosion morphology after 4 h immersion in 0.5 wt% NaCl naturally aerated solution at room temperature: a) ZK40; b) ZK40-CaO; c) ZK40-Gd; d) ZK40-Nd; e) ZK40-Y.

Figure 5 shows the plannar view of the corroded specimens after 4 h immersion in 0.5 wt.% NaCl solution following by the removal of the corrosion products following. Localised corrosion can be separated into three types:

- Micro "craters" of diameter ~1 µm was observed within the grains for all alloys and more pronounced for the ZK40-Y as highlighted in the insert in Figure 5(e);
- Localised corrosion in the shape of "craters" in some grains was observed for all alloys and more observed in the ZK40-CaO;
- Localised corrosion along the intermetallic phases was observed only for the ZK40-Nd, as highlighted in the insert in Figure 5(d).

The plannar view of the corroded specimens after the removal of the corrosion products following 24 h immersion in 0.5 wt.% NaCl solution is shown in Figure 6. For the ZK40 (Figure 6(a)) and ZK40-Gd (Figure 6(c)), the localised corrosion within the grain is observed. The "micro craters" appears to start to coalesce for the ZK40. No significant differences in localised corrosion are noted for the ZK40-CaO alloy compared to 4 h immersion (Figure 5(b)). Severe localised corrosion was observed for the ZK40-Nd (Figure 6(d)) and ZK40-Y (Figure 6(e)) alloys, while it was more pronounced for the ZK40-Nd alloy. In the case of the ZK40-Nd, the corrosion front seems to have started at the grain boundary, and propagate toward the α-Mg matrix (inserted figure in Figure 6(d)). On the other hand, the corrosion front seems to propagate along the grain boundary, without deep corrosion of the α-Mg matrix for the ZK40-Y.

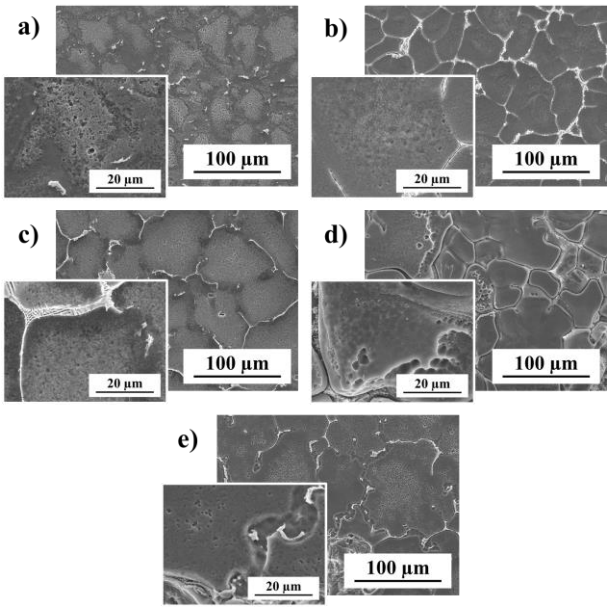

Figure 6. Corrosion morphology after 24 h immersion in 0.5 wt% NaCl naturally aerated solution at room temperature: a) ZK40; b) ZK40-CaO; c) ZK40-Gd; d) ZK40-Nd; e) ZK40-Y.

4.- DISCUSSION.

The as-cast microstructure of the ZK40 alloy was modified with the addition of Ca, Gd, Nd and Y elements. A small volume fraction of intermetallic particles if formed for the ZK40 alloy. The ZK40 with the addition of Ca, Gd, Nd and Y resulted in a semi-continuous network of intermetallic particles along the

grain boundaries. The volume fraction of the intermetallic phases were higher for the ZK40-Nd alloy. Individual particles of CaO was not found in the as-cast microstructure. Wiese et al. [10] who reported CaO disassociates during melting.

The addition of 2 wt.% of Nd to the ZK40 was detrimental to the corrosion resistance. However, the corrosion resistance was slightly improved by Gd and Ca additions. An incubation period with a low rate of hydrogen evolution is followed by a period of acceleration in hydrogen evolution. After ~175 h exposure for the ZK40, ZK40-CaO, ZK40-Gd and ZK40-Y alloys the hydrogen evolution volume reached a near-constant rate of increase. Accelerated corrosion kinetics is observed for the ZK40-Nd.

The intermetallic phases are more noble and more stable than the α-Mg matrix, as reported for Mg-RE (0.5-5% La, 0.5-5% Ce, 0.5-4% Nd) [11], and ZE41 [3], [12]. The immersion tests reveal that corrosion initiate locally in the investigated alloys. The main difference is the kinetics of the localised corrosion within the grain and the corrosion resistance offered by the grain boundaries. For the ZK40, ZK40-CaO and ZK40-Gd alloys the grain boundaries seem to hinder the corrosion front. On the other hand, the corrosion front seems to propagate along the grain boundaries when severe localised corrosion starts for the ZK40-Y. Localised corrosion of the α-Mg matrix at the interface of the intermetallic phase along the grain boundary is observed for the ZK40-Nd after 4 h of immersion. The corrosion front seems to start at the grain boundaries and propagate fast into the grains after 24 h. The intensive localised corrosion and absence of corrosion barriers explain the poor corrosion resistance of the ZK40-Nd.

4.- SUMMARY AND CONCLUSIONS.

The corrosion resistance of the as-cast ZK40 (Mg-4.5Zn-0.6Zr), ZK40 with 2 wt.% of Ca, Gd and Nd and 1 wt.% Y (ZK40-CaO, ZK40-Gd, ZK40-Nd and ZK40-Y, respectively) were investigated. The following conclusion can be drawn:

- The addition of Ca, Gd, Nd and Y modified the as-cast microstructure of the ZK40.
- The corrosion resistance measured by three different techniques was enhanced for the ZK40-CaO and slightly inferior for the ZK40-Y.
- The detrimental effect of Nd addition on the ZK40 alloy is attributed to micro galvanic corrosion.
- The semi-continuous network of intermetallic compounds along the grain boundary hindered the corrosion (barrier effect) and improved the corrosion properties for the ZK40-CaO.
- The area fraction of intermetallic compounds is lower for the ZK40-Y compared to the ZK40-CaO, and the barrier effect does not play an important role, leading to a decrease in the corrosion resistance.

5.- ACKNOWLEDGEMENTS.

RHB would like to acknowledge the CD-Laboratory for Design of High-Performance Alloys by Thermomechanical Processing and the Christian Doppler Forschungsgesellschaft for the financial support.

6.- REFERENCES.

[1] Kainer K. U., “Magnesium alloys and technology”, Weinheim, Wiley-CVH Gmbh & Co. KGaA, 2003.

[2] Yamasaki M., Hayashi N., Izumi S., and Kawamura Y., “Corrosion behavior of rapidly solidified Mg–Zn–rare earth element alloys in NaCl solution,” *Corros. Sci.*, vol. 49, no. 1, pp. 255–262, 2007.

[3] Zhao M.-C., Liu M., Song G. L., and Atrens A., “Influence of Microstructure on Corrosion of As-cast ZE41,” *Adv. Eng. Mater.*, vol. 10, no. 1-2, pp. 104–111, 2008.

[4] Wu G., Fan Y., Gao H., Zhai C., and Zhu Y. P., “The effect of Ca and rare earth elements on the microstructure, mechanical properties and corrosion behavior of AZ91D,” *Mater. Sci. Eng. A*, vol. 408, no. 1, pp. 255–263, 2005.

[5] Zhang T., Meng G., Shao Y., Cui Z., and Wang F., Corrosion of hot extrusion AZ91 magnesium alloy. Part II: Effect of rare earth element neodymium (Nd) on the corrosion behavior of extruded alloy,” *Corros. Sci.*, vol. 53, no. 9, pp. 2934–2942, 2011.

[6] Yang M., Cheng L., and Pan F., “Comparison about effects of Ce, Sn and Gd additions on as-cast microstructure and mechanical properties of Mg–3.8Zn–2.2Ca (wt%) magnesium alloy,” *J. Mater. Sci.*, vol. 44, no. 17, pp. 4577–4586, 2009.

[7] Mandal M., Moon A. P., Deo G., Mendis C. L., and Mondal K., “Corrosion behavior of Mg–2.4Zn alloy micro-alloyed with Ag and Ca,” *Corros. Sci.*, vol. 78, pp. 172–182, 2014.

[8] Jeong Y. S., and Kim W. J., “Enhancement of mechanical properties and corrosion resistance of Mg–Ca alloys through microstructural refinement by indirect extrusion,” *Corros. Sci.*, vol. 82, pp. 392–403, 2014.

[9] Elsayed F. R., Hort N., Salgado-Ordorica M. A., Kainer K. U., “Magnesium Permanent Mold Castings Optimization”, *Mat. Sci. Forum* vol. 690, pp. 65-68, 2011.

[10] Wiese B., Mendis C.L., Tolnai D., Stark A., Schell N., Reichel H.-P., Brückner R., Kainer K.U., Hort N., “CaO dissolution during melting and solidification of a Mg–10wt.% CaO alloy detected with in situ synchrotron radiation diffraction,” *J. Alloys Compd.*, vol. 618, pp. 64–66, 2015.

[11] Birbilis N., Easton M. A., Sudholz A. D., Zhu S. M., and Gibson M. A., “On the corrosion of binary magnesium-rare earth alloys,” *Corros. Sci.*, vol. 51, no. 3, pp. 683–689, 2009.

[12] Zhao M.-C., Liu M., Song G.-L., and Atrens A., “Influence of pH and chloride ion concentration on the corrosion of Mg alloy ZE41,” *Corros. Sci.*, vol. 50, no. 11, pp. 3168–3178, 2008.